Analytica Chimica Acta 1226 (2022) 340251

Contents lists available at ScienceDirect

Analytica Chimica Acta

journal homepage: www.elsevier.com/locate/aca

Construction of electrochemiluminescence biosensor for monitoring of glutathione released by living cancer cells

Jinzha Zhang, Xuan Liu, Huaxiao Liu, Jingzhi Wang, Yawen Zhang, Wenbo Zhao *

National and Local Joint Engineering Research Center of Biomedical Functional Materials, School of Chemistry and Materials Science, Nanjing Normal University, Nanjing, 210023, PR China

HIGHLIGHTS

- Hypotoxic $AgGaS_2/SiO_2$ nanoparticles were prepared by thermal decomposition and reverse microemulsion method.
- The ECL biosensor can sensitively detect GSH released by living cancer cells.
- The proposed ECL biosensor platform showed excellent stability, satisfactory selectivity and reproducibility for GSH detection.

GRAPHICAL ABSTRACT

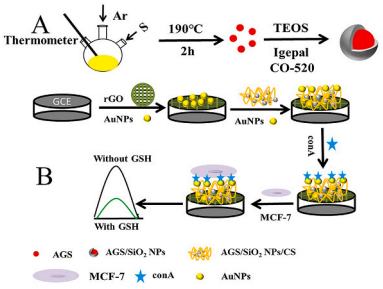

ARTICLE INFO

Keywords:
$AgGaS_2$ quantum dots
Electrochemiluminescence biosensor
Glutathione detection
Live cancer cells

ABSTRACT

Abnormal glutathione (GSH) levels are directly related to specific diseases. Therefore, the highly sensitive detection of GSH has attracted extensive attention of researchers. Here, we reported a novel electrochemiluminescence (ECL) biosensor platform based on $AgGaS_2$ quantum dots (AGS QDs) for sensitive detection of GSH released by living cancer cells. Firstly, the preparation and photoluminescence of AGS QDs were studied. Then, ECL biosensor based on AGS QDs was constructed and applied to the detection of GSH released by MCF-7 cells. The experimental results showed that the ECL biosensor can sensitively detect GSH directly released by living cancer cells *in situ*. This work not only provides a promising choice for developing ECL with low toxicity and good biocompatibility, but also can be extended to detect other molecules released by cells, which is conducive to the in-depth study of pathophysiology.

1. Introduction

Glutathione (GSH) is a tripeptide containing sulfhydryl groups, which is formed by the combination of glutamate, cysteine and glycine, and widely exists in animals. As an important metabolic substance in the body, it participates in the tricarboxylic acid cycle and glucose metabolism, and can activate a variety of enzymes to promote the metabolism of sugars, fats and proteins [1]. It also participates in many important biochemical reactions [2]. Based on its antioxidant properties, it can remove free radicals and toxins, protect the sulfhydryl groups of important enzyme proteins from oxidation and inactivation, so as to ensure the normal play of molecular physiological functions such as proteins and enzymes [3]. Abnormal GSH levels in the body are directly related to specific diseases, including cancer, human immunodeficiency

* Corresponding author.
E-mail address: zhaowenbo@njnu.edu.cn (W. Zhao).

https://doi.org/10.1016/j.aca.2022.340251
Received 12 December 2021; Received in revised form 26 July 2022; Accepted 8 August 2022
Available online 11 August 2022

virus, liver injury and neurodegenerative diseases [4–6]. Therefore, the level of GSH is very important for *in vivo* detection and biological diagnosis system.

The level of GSH (2–10 mM) in cytoplasm is much higher than that in extracellular matrix (ECM) (2–20 μM). In tumor tissues, especially in multidrug resistant (MDR) tumors, GSH in cytoplasm is four times higher than that in healthy tissues [7]. At present, researchers have proposed a variety of methods to detect GSH or monitor the changes of GSH in cells, including enzyme-linked immunosorbent assay, surface enhanced Raman scattering, high performance liquid chromatography (HPLC) and mass spectrometry [8–11]. However, these traditional detection methods are often complex, expensive and time-consuming. Electrochemiluminescence (ECL) method is famous for its super sensitivity, near zero background response, wide dynamic range, simplified optical setting and no external light source. It is a recognized as a multifunctional analytical technology in the fields of life analysis, drug research and environmental monitoring [12–17]. Recently, this method has also been applied to the detection of GSH. For example, Shan et al. used ferrocyanide ferrocyanide redox pair to amplify the ECL signal of carbon quantum dots to sensitively detect GSH [18]. Han et al. applied ECL hydrogel system to detect GSH in serum [19]. Based on the Au nanoclusters/Cu_2O heterostructure, Yuan et al. manufactured a feasible ECL biosensor for ultrasensitive determination of GSH in solution [20]. However, so far, there has been no study on ECL detection of GSH released directly from living cells, which has important theoretical research value for the distribution and metabolism of GSH *in vivo*.

Here, we are committed to the construction and application of an ECL biosensors for monitoring GSH release from living cancer cells. Among them, the construction of ECL biosensor becomes the key to detection. The performance of ECL signal probe is very important to improve the analytical performance of ECL sensing platform. With the progress of ECL technology, various ECL emitters with excellent performance have been applied to ECL analysis platform, such as organic molecules, two-dimensional (2D) nanosheets, metal oxides and quantum dots [21–26]. Binary II-VI nanocrystals (NCs) have the advantages of high luminous efficiency, good stability and size-adjustable photoluminescence. They are considered to be promising ECL emitters, but they also have obvious disadvantages, that is, there are toxic elements in their components, such as cadmium (Cd) and plumbum (Pb) [27–29], which is obviously not conducive to their application in the detection of metabolites in cell system. Therefore, it is of great significance to develop non-toxic and heavy metal-free luminescent nanomaterials as ECL phosphors. In recent years, the emergence of ternary I-III-VI_2 NCS as new non-toxic and light stable luminescent nanomaterials has provided the possibility to replace the II-VI NCS in the development of ECL emitters [30–34].

Bulk $AgGaS_2$ with a direct band gap of 2.5–2.7 eV in I-III-VI semiconductors has unique optical nonlinearity and bi-refringence characteristics [35–40]. Here, we designed and constructed an ECL sensor based on $AgGaS_2$ quantum dots (AGS QDs) (Scheme 1). Firstly, AGS QDs were synthesized by thermal decomposition method. AGS QDs showed near-infrared fluorescence emission, with a maximum emission wavelength of about 820 nm and a red-shift of about 170 nm. In order to improve the biocompatibility and water dispersion of AGS QDs, a layer of silica was coated on the surface of AGS QDs, and then AGS/SiO_2 NPs were fixed on the surface of glassy carbon electrode (GCE) with chitisan (CS), and doped with gold nanoparticles (Au NPs) and reduced graphene oxide (rGO) nanomaterials. Au NPs and rGO nanomaterials can improve the conductivity of the electrode. The former can also be used to fix Con A protein, which can recognize the glycosyl chain on the surface of cancer cells MCF-7 to capture cancer cells [41]. When $K_2S_2O_8$ was used as a co-reactant, AGS/SiO_2 NPs had a strong ECL signal. GSH has significant reduction characteristics and $K_2S_2O_8$ has strong oxidation characteristics. When the tested object GHS interfered with $K_2S_2O_8$, the ECL signal decreased, so a new ECL biosensor platform was constructed and its performance was studied in detail.

2. Experimental section

2.1. Preparation of $AgGaS_2$ QDs

Firstly, 0.25 mmol of gallium acetylacetonate, 0.25 mmol of silver acetate, 4 mL of 1-octadecene, and 1 mL of oleic acid were added into a 25 mL three-neck flask. Then, the mixed solution was heated to 110 °C under argon protection for 30 min. Subsequently, the above solution was injected with 0.5 mL of dodecyl mercaptan (DDT), until the solution

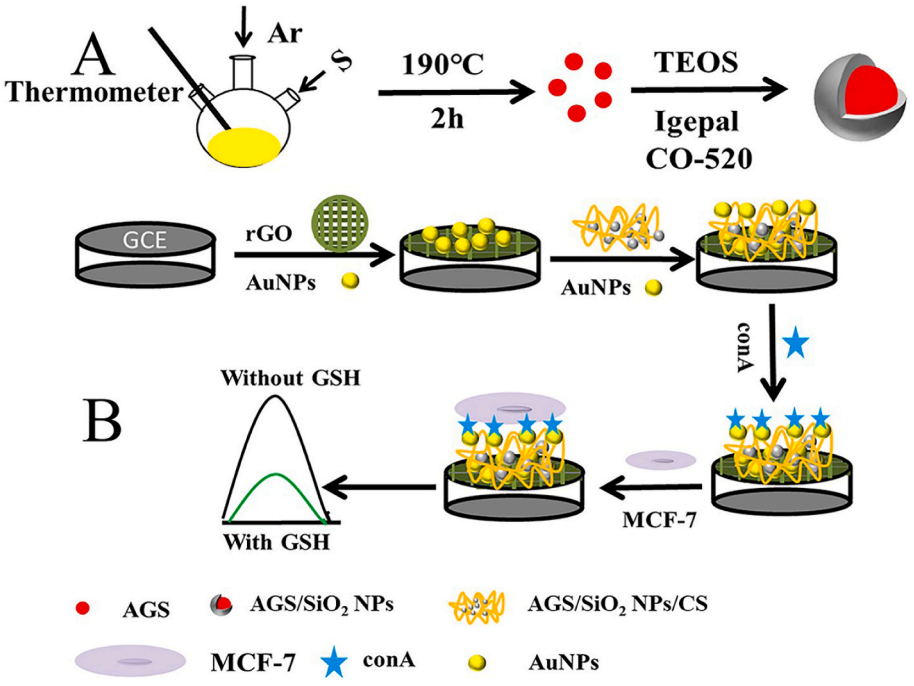

Scheme 1. Schematic illustration for (A) Preparation of AGS/SiO_2 NPs, and (B) Fabrication procedures of ECL biosensor for cell assay.

turned bright yellow. Under an argon atmosphere, the reaction mixture was stirred and heated to 190 °C. 0.05 mmol of sulfur powder was added into 1 mL oleylamine solution to form sulfur precursor solution. The sulfur precursor solution was injected into the above reaction mixture when the solution temperature stabilized and formed orange solution. The solution darkened immediately after injection and reacted for another 2 h. After the reaction was cooled to room temperature, ethanol and cyclohexane were added to the mixture, and the colloidal quantum dot solution was centrifuged at 8000 rpm for 8 min. After repeated cleaning for 3 times, and the obtained $AgGaS_2$ QDs were dried in a vacuum oven at 60 °C and stored at room temperature.

2.2. Preparation of $AgGaS_2/SiO_2$ NPs (AGS/SiO_2 NPs)

The AGS/SiO_2 NPs were prepared by the reverse microemulsion method (Scheme 1A). First, 2 mg of AGS QDs were dissolved in 12 mL cyclohexane by ultrasonication. Next, 700 μL of IGEPAL-50, 400 μL of ammonia, and 30 μL tetraethyl orthosilicate (TEOS) were added simultaneously to the above solution. The reaction temperature was maintained at 28 °C for 20 h 10 μL methanol was added to the above solution at the end of the reaction to disrupt a reverse microemulsion. Subsequently, the silica-coated AGS QDs were collected by centrifugation and washed twice with ethanol and double-distilled water. Finally, the AGS/SiO_2 NPs were dispersed in 2 mL of double distilled water and stored in a refrigerator at 4 °C for later use.

2.3. Assembly of ECL biosensor

The biosensor was constructed as shown in Scheme 1B. Before preparing the working electrode, 0.05 μM alumina powder was used to polish GCE (3 mm), then washed and ultrasonic treated in ethanol and ultrapure water to remove surface impurities and dried with nitrogen for further use. GCE was placed in 6 mL of graphene oxide dispersion (GO), and the scanning voltage was set to 0 ~ −1.5 V for 5 turns to reduce GO to rGO, deposited it on the electrode surface to obtain GCE/rGO, and the unreduced GO was washed with PBS solution and then dried in an oven at 37 °C. Next, GCE/rGO was placed into 6 mL $HAuCl_4$ (2%) solution, and GCE/rGO/Au NPs were obtained by cyclic voltammetry (the scanning cycles from - 0.8 V to + 0.2 V, at a scan rate of 100 mV s^{-1}), and the unreduced Au NPs were rinsed with washing buffer. After drying at 37 °C, the working electrode was covered with 10 μL of the pre-prepared AGS/SiO_2 and chitosan (CS) mixture (5: 1 (v/v)) and dried at room temperature. Then the electrode was cleaned with 0.01 M sodium hydroxide solution and ultrapure water and dried to obtain GCE/rGO/Au NPs/AGS/SiO_2/CS. Subsequently, GCE/rGO/Au NPs/AGS/SiO_2/CS was immersed in 6 mL of $HAuCl_4$ (2%) solution to prepare Au NPs that can be used for Con A protein immobilization and washed unreduced Au NPs with PBS solution for 2 times, and further dried. 10 μL Con A (2 mg mL^{-1}) was then added dropwise to the surface of the above-modified electrode and dried for 1.5 h to obtain GCE/rGO/AuNPs/AGS/SiO_2/CS/AuNPs/ConA. Finally, the modified GCE was washed with PBS and stored in a refrigerator at 4 °C for subsequent use.

2.4. Cell culture

MCF-7 cancer cells were obtained from the Chinese Academy of Sciences cell bank (Shanghai, China) and cultured in a high-glucose DMEM supplemented containing 10% Fetal Bovine Serum (FBS) at 37 °C and 5% CO_2 environment. Subsequently, the cells grown at a density of about 80% adnexal to the wall were digested with trypsin to make a cell suspension and diluted with PBS (100 000 cells mL^{-1}).

2.5. Assay of GSH

Different concentrations of GSH solution were mixed with 0.1 M PBS solution (pH 7.4) containing 50 mM $K_2S_2O_8$, respectively. Then the electrode was placed in the mixed solution to detect the change of ECL signal. ECL method was used to detect GSH released by MCF-7 cells *in situ*. 10 μL of the diluted cell suspension was dropped onto the prepared electrode and incubated it in a cell incubator at 37 °C and 5% CO_2 for 40 min. Next, the electrode was taken out and washed with 0.1 M PBS solution to remove unattached cells and placed in the above solution for GSH assay. After reaching a steady ECL intensity from the GCE/rGO/AuNPs/AGS/SiO_2/CS/AuNPs/ConA/cells, 10 μL of n-ethylmaleimide (NMM, 100 μg mL^{-1}) was injected into the cells in advance to inhibit GSH production and then placed in a solution for GSH detection.

2.6. Fluorescence quantum yield calculation

The following equation calculated the fluorescence quantum yield (QY) of AGS QDs (dissolved in cyclohexane) with the quantum yields of known standard reference solutions (rhodamine B dissolved in ethanol).

QY sample = QY rhodamine B {I sample/I standard} {n_2 sample/n_2 standard};

I is the ratio of the integrated area of the fluorescence peak to the UV absorption intensity, where n is the refractive index of the solvent [42].

3. Results and discussion

3.1. Characterization of AGS QDs and AGS/SiO_2 NPs

The optical properties of AGS QDs were presented in fluorescence emission spectra and UV–vis absorption spectra (Fig. 1). The maximum fluorescence emission peak of AGS QDs was about 820 nm and the maximum half-peak width was less than 150 nm (Fig. 1A). The fluorescence QY of AGS QDs was calculated to be 7.99%. Furthermore, AGS QDs were analyzed by UV–vis absorption spectra (Fig. 1B). It could be seen that the absorption peak of AGS QDs was a broad-shouldered peak with no obvious excite peak [43]. The XRD pattern was used to verify the phase and structure of the obtained AGS QDs sample (Fig. S1). The test results were compared with the XRD of the AGS QDs standard card (JCPDS NO.65-1574). It could be seen that all the diffraction peaks matched the standard card [44], indicating that the AGS QDs were successfully prepared.

Energy dispersive spectroscopy (EDS) of AGS QDs exhibited peaks related to three elements of Ag, Ga, and S (Fig. S2). The content ratios of the three elements were 24.94%, 20.71%, and 54.35%, respectively. The ratio of each element was about 1: 1: 2, which further proved that AGS QDs were successfully prepared.

X-ray photoelectron spectroscopy (XPS) was carried out to analyze the chemical composition and elemental valence states of AGS QDs. The high-resolution peak-fitting XPS spectra were used to analyze Ag 3d, Ga 2p, and S 2p. Ag, Ga, S, N, O, and C elements can be observed in the full spectrum of XPS (Fig. S3A). The existence of N, O, and C elements may be attributed to the elements carried by oleylamine and oleic acid ligand groups on the surface of the quantum dots. Next, 3d peaks of Ag were analyzed (Fig. S3B). The peaks of 3d3/2 and 3d5/2 were 373.83 eV and 367.78 eV, respectively, which were consistent with the reference value of Ag(I), thus demonstrating that the chemical valence of Ag was +1 valence. The 2p orbital analysis of Ga (Fig. S3C) and the peaks of 2p1/2 and 2p3/2 were 1144.83 eV and 1118.03 eV, respectively, indicating the chemical valence of Ga was +3 valence. The 2p spectrum of S showed that its peak position was fitted by two peaks of 162.23 eV and 161.28 eV. The double peaks corresponded to 2p1/2 peak and 2p3/2 peak of S, and its chemical valence was −2 (Fig. S3D). The results showed that AGS QDs were successfully synthesized.

The TEM image of the synthesized organic phase AGS QDs showed that the AGS QDs had good dispersion, with an average diameter of about 4 nm (Fig. 2A), which may contribute to the electron transfer in the electroluminescence process. The HRTEM image (inset Fig. 2A) demonstrated that AGS QDs had a good crystalline shape. AGS/SiO_2 NPs were prepared by using the reverse microemulsion method. It was found

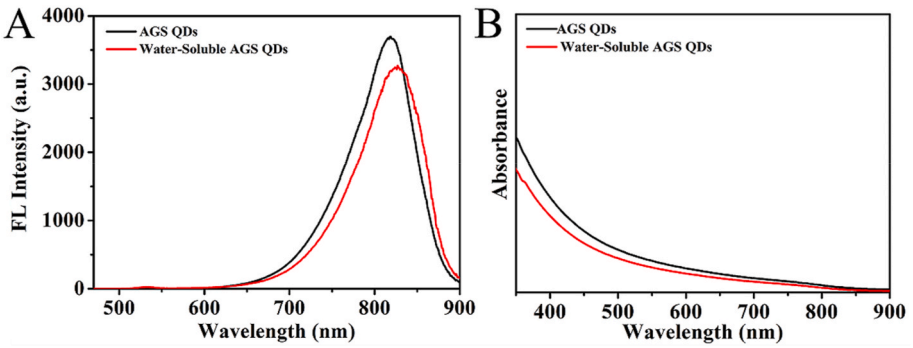

Fig. 1. (A) Fluorescence and (B) UV–vis absorption spectra of AGS QDs.

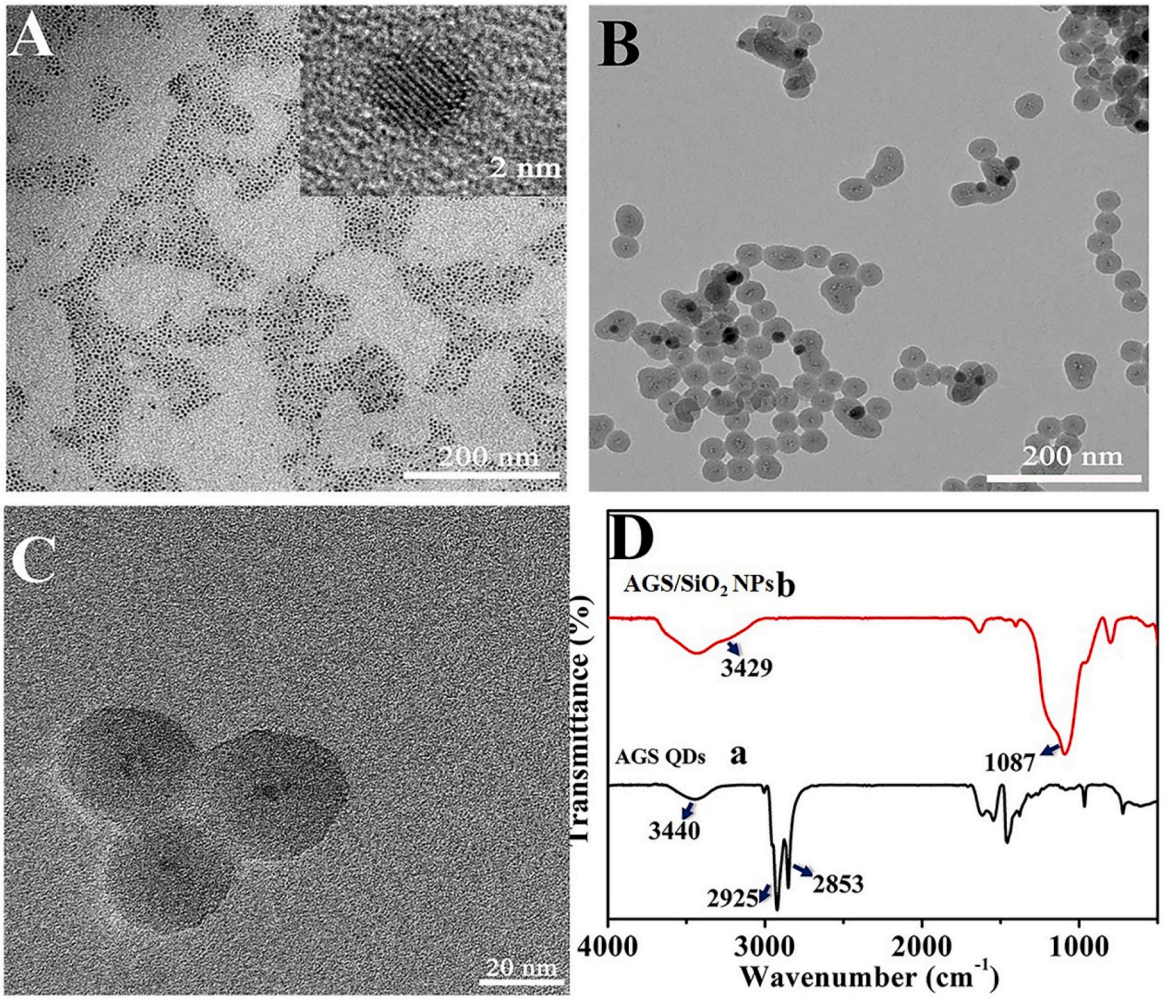

Fig. 2. TEM image and HRTEM image (A) $AgGaS_2$ QDs; (B) TEM image of AGS/SiO_2 NPs; (C) HRTEM image of AGS/SiO_2 NPs; (D) FTIR spectra of AGS QDs and AGS/SiO_2 NPs.

that silica was successfully wrapped the quantum dots with the average particle diameter of about 30 nm (Fig. 2B). The quantum dots were located in the center of the silica shell, indicating that the silica shell grew in an anisotropic direction. Subsequently, AGS/SiO_2 NPs morphology was further analyzed by the HRTEM (Fig. 2C), which further proved successful parcels of silica coating.

AGS QDs were characterized by FTIR spectra (Fig. 2D, curve a). Firstly, a strong broad peak at 3400 cm^{-1} can be attributed to the stretching vibration of –OH or $–NH_2$ bond of AGS QDs, which may result from the group carried by oleic acid or oleylamine ligand on the surface of quantum dots. Secondly, two strong peaks at 2853 cm^{-1} and 2925 cm^{-1} belonged to the asymmetric and symmetric stretching vibrations of $–CH_2$, respectively. In addition, the –OH (3429 cm^{-1}), Si–O (1087 cm^{-1}) stretching vibration of SiO_2 were observed, showing that SiO_2 was successfully attached to the surface of the AGS QDs (Fig. 2D, curve b). The introduction of hydroxyl group may bring good hydrophily and biocompatibility. We also explored the effect of the concentration of AGS QDs on the formation of SiO_2 shells (Fig. S4). TEM image showed that when 0.083 mg mL^{-1} AGS QDs were consumed, many silica nanoparticles without quantum dots were formed (Fig. S4A). When the

concentration of quantum dots increased to 0.25 mg mL^{-1}, a large amount of SiO_2 shells were connected into thin sheets, and the shape of silicon shells was irregular (Fig. S4C). This phenomenon was similar to the results previously reported in literature [45]. Therefore, we speculated that the formation of SiO_2 shells was related to the concentration of AGS QDs. In this case, the optimal concentration of AGS/SiO_2 NPs was 0.167 mg mL^{-1} (Fig. S4B). *3.2. Research of ECL properties of AGS/SiO_2 NPs.*

The ECL properties of AGS/SiO_2 NPs were examined. The cathode ECL of AGS/SiO_2 NPs was investigated in the presence of $K_2S_2O_8$, a typical co-reactant for cathodic ECL of NPs. The ECL responses and cyclic voltammetry (CV) characterization of NPs were carried out at the scan range of 0 to −2 V within a scan rate of 100 mV s^{-1}, which was in a PBS (pH 7.4) solution, including 0.1 M KCl without and with 50 mM $K_2S_2O_8$. As expected, there was almost no related reduction peak of CV curve (Fig. 3A, curve a) and no noticeable ECL emissions (Fig. 3B, curve a) can be observed on GCE/AGS/SiO_2 NPs in the absence of $K_2S_2O_8$ as a co-reactant. After adding 10 mM of $K_2S_2O_8$, obvious ECL emission (Fig. 3B, curve b) and reduction peak potentials of −0.8 V and −1.2 V in CV curve (Fig. 3A, curve b) were observed. This may be due to the electrochemically oxidized $K_2S_2O_8$ and AGS/SiO_2 NPs participated in ECL of the co-reactant. Simultaneously, the ECL responses of GCE/AGS/SiO_2 NPs showed many reproducible signals during a continuous potential sweep (Fig. 3C), indicating that the proposed ECL system had excellent stability.

The strong co-reactant ECL demonstrated that radiative charge transfer in GCE/AGS/SiO_2 NPs could also be readily achieved at the cathode in the co-reactant route by simultaneously injecting both holes and electrons into AGS/SiO_2 NPs. The reaction mechanism can be explained as follows:

$$S_2O_8^{2-} + e^- \rightarrow SO_4^{2-} + SO_4^{\bullet-} \quad (1)$$

$$AGS/SiO_2 + e^- \rightarrow AGS/SiO_2^{\bullet-} \quad (2)$$

$$AGS/SiO_2^{\bullet-} + SO_4^{\bullet-} \rightarrow AGS/SiO_2{}^* + SO_4^{2-} \quad (3)$$

$$AGS/SiO_2{}^* \rightarrow AGS/SiO_2 + h\nu \quad (4)$$

The cathode co-reactant $K_2S_2O_8$ obtained an electron at the cathode to form SO_4^{2-} and $SO_4^{\bullet-}$, and similarly AGS/SiO_2 NPs received an electron to form the unstable AGS/$SiO_2^{\bullet-}$, which had a strong reducing $SO_4^{\bullet-}$ interacted with AGS/$SiO_2^{\bullet-}$ to form the excited state AGS/SiO_2*, which returned to the ground state after relaxation to produce the ECL signal. Similarly, we explored another common cathode co-reactant, H_2O_2, which also had a reduction peak at −1.42 V (Fig. S5A, curve b), but did not produce a strong ECL signal (Fig. S5B, curve b). Therefore, we speculated that the strongly oxidized radical generated by H_2O_2 cannot interacted with AGS/SiO_2 to generate stable excited state of AGS/SiO_2*, which returned to the ground state after relaxation produces a weaker ECL signal. Meanwhile, we also explored the anode co-reactants TPrA and $Na_2C_2O_4$. The CV curve showed that both TPrA and $Na_2C_2O_4$ had an oxidation peak with peak positions at 1.03 V (Fig. S5C, curve b) and 1.47 V (Fig. S5E, curve b), respectively. At the same time, no obvious ECL signal was observed (Figs. S5D and S5F). Therefore, we speculated that the reason for weaker ECL signals generated by the interaction of TPrA and $Na_2C_2O_4$ with AGS/SiO_2 NPs was similar to that of H_2O_2 and AGS/SiO_2 NPs.

3.2. ECL quenching mechanism of AGS/SiO_2 NPs by GSH

GSH (R–SH) can exert its antioxidant properties due to the reactivity of sulfhydryl groups. Therefore, it is obvious that the reaction of sulfhydryl groups with $SO4^{\bullet-}$would hinder the radiative recombination of electrons and holes captured on the surface of AGS/SiO_2 NPs, resulting in ECL quenching of the proposed biosensor [46]. The possible quenching mechanism was as follows (Scheme S1):

$$SO_4^{\bullet-} + R\text{–}SH + OH^- \rightarrow R\text{–}S^{\bullet} + SO_4^{2-} + H_2O \quad (5)$$

$$R\text{–}S^{\bullet} + R\text{–}S^{\bullet} \rightarrow R\text{-}S\text{-}S\text{-}R \quad (6)$$

3.3. ECL property of different biosensors

Next, we studied the ECL behavior of different modified GCE. The ECL intensity of GCE/AGS/SiO_2/CS was lower than that of GCE/AGS/SiO_2 NPs (Fig. S6A, curve b and a), due to the steric hindrance of CS that hindered the electron transfer. However, the ECL intensity of GCE/rGO/AuNPs/AGS/SiO_2/CS was 3 times higher than that of GCE/AGS/SiO_2/CS because rGO had a large specific surface area, which can adsorb more AuNPs to improve the electrical conductivity of electrode (Fig. S6A, curve c).

3.4. Optimization of experimental conditions

In order to obtain a satisfactory ECL biosensing platform, some essential experimental parameters were optimized, such as scanning rate and solution pH. The influence of the scan rate on the ECL intensity was shown in Fig. S7A. When the scan rate was lower than 100 mV s^{-1}, the ECL intensity increased with the increase of the scan rate, but then dropped sharply at a scan rate higher than 100 mV s^{-1}. As a consequence, 100 mV s^{-1} was the optimal scan rate to achieve high ECL intensity of biosensor. Simultaneously, the effect of the pH value of buffer solution on the ECL intensity of biosensor was shown in Fig. S7B. In the range of pH from 4.0 to 7.0, the ECL intensity increased significantly and reached a plateau at pH 7.0, and then began to decline. Therefore, the reaction condition of pH 7.0 was adopted in subsequent experiments. Moreover, we also analyzed the incubation time and incubation temperature of MCF-7 cells, and obtained the optimal incubation time and incubation temperature were 40 min (Fig. S8A) and 37 °C (Fig. S8B), respectively.

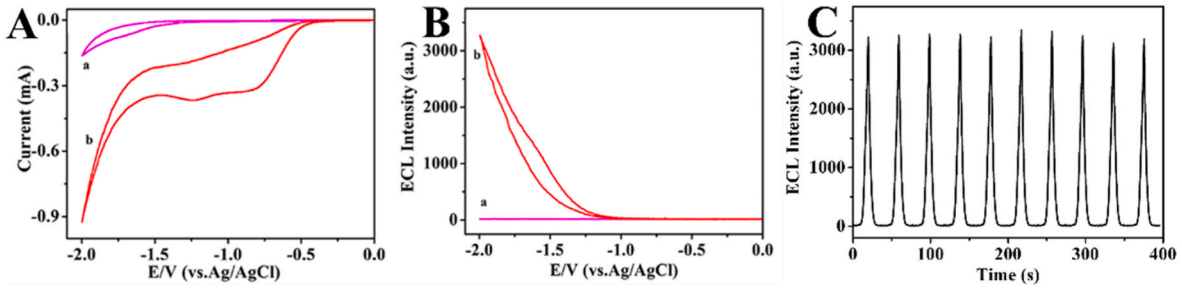

Fig. 3. (A) Cyclic voltammetry; (B) ECL intensity-potential response plots of GCE/AGS/SiO_2 NPs in 0.1 M PBS (pH 7.4) solution, containing 0.1 M KCl (a) without or (b) with 50 mM $K_2S_2O_8$; (C) Stability of ECL signals of AGS/SiO_2 NPs in 0.1 M PBS (pH 7.4) containing 0.1 M KCl with 50 mM $K_2S_2O_8$.

3.5. ECL response of the GCE/rGO/AuNPs/AGS/SiO_2/CS to GSH

Based on the best experimental conditions, the GCE/rGO/AuNPs/AGS/SiO_2/CS sensor was exploited to determine GSH of sample. The ECL response was measured by changing GSH concentration of sample. Fig. 4A showed that the ECL intensity decreased with the increase of GSH concentration. Moreover, the change of ECL signal ΔI ($\Delta I = I - I_{GSH}$) had a linear relationship with the logarithmic value of GSH concentration. The linear regression equation for the GSH concentration range of 10 pM–1 μM was $I = 328.89\ lgC + 3851.36$ with a correlation coefficient of 0.995 (Fig. 4B). At 1 μM–10 mM, the linear regression equation was $I = 599.2\ lgC + 5537.8$ with a correlation coefficient of 0.994. The detection limit was calculated to be 8.03×10^{-12} M (S/N = 3) (Fig. 4C). What's more, various interfering substances such as reactive molecules (L-Cys, L-Thr , L-Arg, L-Glu , L-Pro) and metal ion Na^+ , K^+, Ca^{2+}, Mg^{2+} were applied to survey the anti-interference ability of the biosensor. As shown in Fig. 4D, compared with 1 nM GSH, the concentration of L-Cys, L-Thr, L-Arg, L-Glu, L-Pro, Na^+ , K^+, Ca^{2+}, and Mg^{2+} up to 1 μM didn't cause any observable ECL signal, implying the proposed ECL biosensor had excellent selectivity.

3.6. Detection of GSH released from living cancer cells

The proposed biosensor was constructed by a self-assembly method for the detection of GSH released from living cancer cells. CV plots of different modified electrodes in 5.0 mM $K_3[Fe(CN)_6]/K_4[Fe(CN)_6]$ in PBS (0.1 M, pH 7.0) solution with 0.1 M KCl was used to characterize the electrochemical performance of the biosensor. We deposited rGO, AuNPs by electrodeposition to enhance the conductivity of the coating, then the current strength was significantly enhanced (Fig. 5A, curve b). When AGS/SiO_2/CS was decorated on GCE, the current intensity decreased due to the hindrance of the material (Fig. 5A, curve c), but its ECL signal was enhanced due to the addition of the ECL luminophores material (Fig. 5B, curve c). Then Con A protein was used for modification. It was a non-conductive biomaterial, which hindered the transfer rate of electrons on the electrode, so the ECL signal (Fig. 5B, curve d) and current intensity (Fig. 5A, curve d) were weakened. The current intensity decreased after modifying MCF-7 cells (Fig. 5A, curve e). As MCF-7 cancer cells released GSH, the corresponding ECL signal was decreased significantly, which may be attributed to the reaction of GSH with $K_2S_2O_8$ (Fig. 5B, curve). The above characterization further demonstrated the successful biosensor assembly. Furthermore, the MCF-7 cells were first captured on the surface of GCE/rGO/AuNPs/AGS/SiO_2/CS/AuNPs/ConA. Then, NMM, as one of the GSH inhibitor, was used to stimulate MCF-7 cells. As shown in Fig. 5C, in the absence of NMM, GCE/rGO/AuNPs/AGS/SiO_2/CS/AuNPs/ConA/cell showed a relatively low ECL signal (Fig. 5C, curve a), while an enhanced ECL signal was observed upon the injection and stimulation by NMM (Fig. 5C, curve b). We speculated that the addition of NMM can inhibit the production of GSH and reduce the attenuation of ECL signal.

The above experimental results showed that the ECL biosensor based on AGS/SiO_2 NPs can be used to detect GSH released by living cancer cells *in situ*. In addition, it is obvious from Table 1 that our method showed better performance in determining GSH than other reported methods.

4. Conclusion

To sum up, we synthesized ternary AGS QDs with near-infrared fluorescence emission by thermal decomposition method for the first

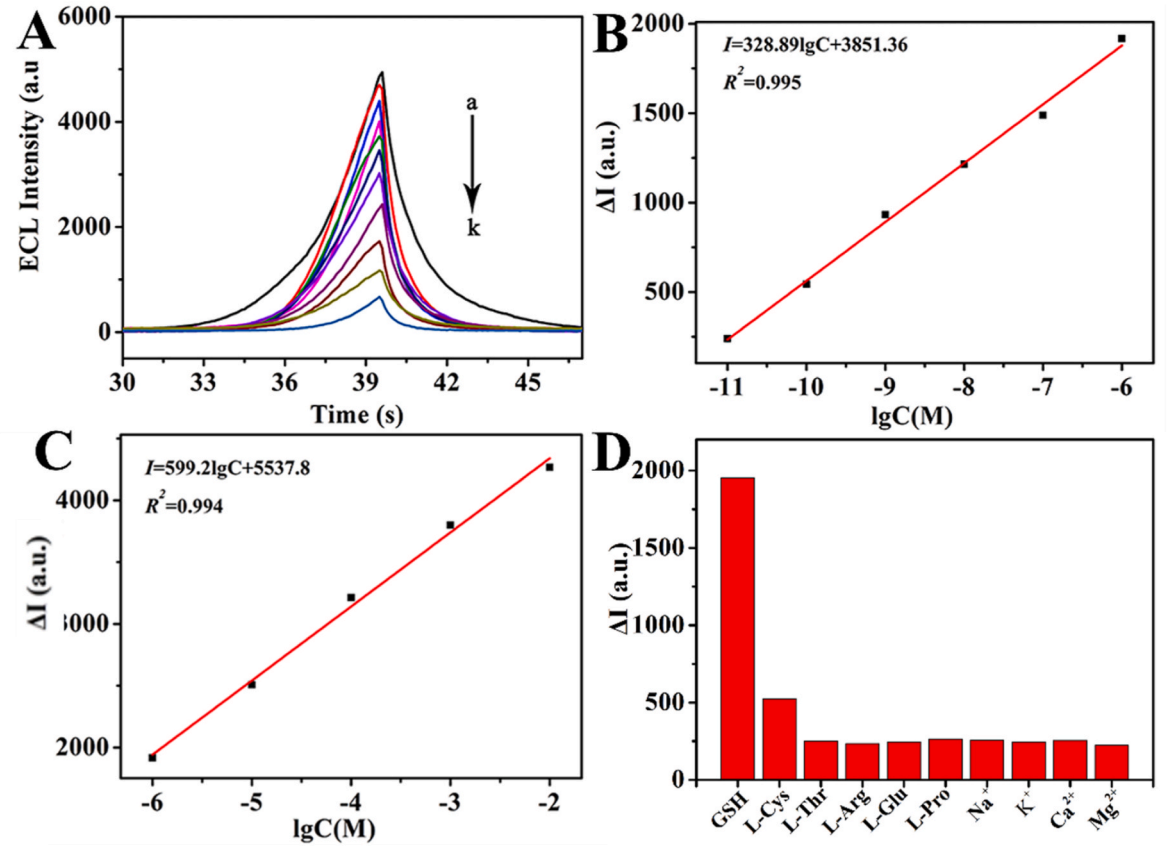

Fig. 4. (A) ECL intensity-time curves for different concentrations of GSH, calibration chart between ECL intensity and lgC_{GSH}; (B) 10 pM–1 μM; (C) 1 μM–10 mM, (a) 0, (b) 10 pM, (c) 100 pM, (d) 1 nM, (e) 10 nM, (f) 100 nM, (g) 1 μM, (h) 10 μM, (i) 100 μM, (j) 1 mM, (k) 10 mM; (D) Selectivity study of GCE/rGO/AuNPs/AGS/SiO_2/CS in 0.1 M PBS (pH 7.0) solution with 50 mM $K_2S_2O_8$ and 0.1 M KCl.

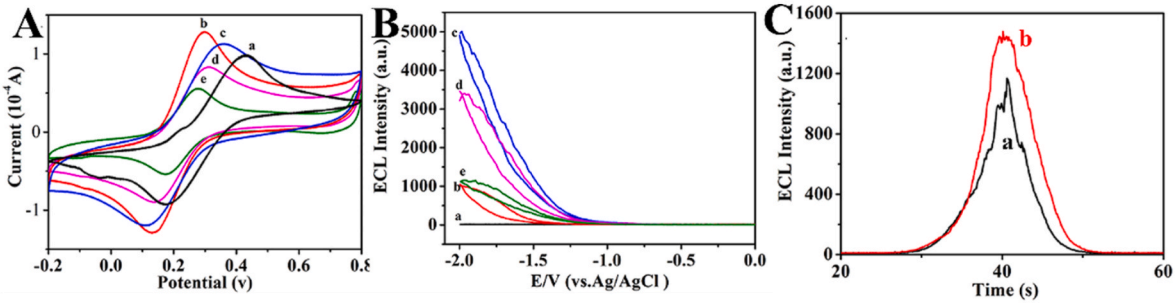

Fig. 5. (A) CV diagram of different modified GCEs in 0.1 M PBS (pH 7.4) solution with 5.0 mM K_3[Fe $(CN)_6$]/K_4[Fe $(CN)_6$] and 0.1 M KCl (Frequency range, 0.1 Hz ~ 100 000 Hz, amplitude, 5 mV); (B) ECL signal response plots with different modified electrodes in 0.1 M PBS (pH 7.0) including 50 mM $K_2S_2O_8$ and 0.1 M KCl solutions (a) bare GCE; (b) GCE/rGO/AuNPs, (c) GCE/rGO/AuNPs/AGS/SiO_2/CS/AuNPs, (d) GCE/rGO/AuNPs/AGS/SiO_2/CS/AuNPs/ConA.

Table 1
Performance comparison of different ways in GSH determination.

Method	Material system	Linear range (μM)	LOD (μM)	Ref.
Fluorescence	Au NCs	50–1.6 × 10^3	0.2	[47]
Fluorescence	EMD NSs[a]	0–2.0 × 10^3	0.28	[48]
Fluorescence	GO-MnO_2	10–2.0 × 10^3	1.53	[49]
ECL	Pt/MnO_2 NF	0.1–10	0.05	[50]
ECL	H-SQDs/MnO_2 NSs	0.05–5.0	0.03	[51]
ECL	AuNC/GCE	1.0 × 10^{-3}-10 10–1.0 × 10^5	3.2 × 10^{-4}	[52]
ECL	Ir (III) –Cu (II) complex	20–80	2.0	[53]
ECL	AGS QDs	1.0 × 10^{-5}- 1.0 1.0–1.0 × 10^4	8.03 × 10^{-6}	This work

[a] EMD NSs: DOX-loaded bacterium/MnOx-based nanospindles.

time. AGS/SiO_2 NPs were then prepared by reverse microemulsion method. Using AGS/SiO_2 NPs as ECL emitter, a high-sensitivity ECL biosensor was constructed to detect GSH. The change of electron-transfer resistance during continuous assembly confirmed the successful construction of ECL biosensor. Experiment results also showed that the biosensor can be used for high sensitivity detection of GSH released by MCF-7 cells. More importantly, it showed the high stability, repeatability and reproducibility required by ECL sensing platform. The sensor has potential application prospects in the detection and treatment of GSH related diseases, and can also be extended to detect other molecules released by cells.

Notes

The authors declare no conflict of interest.

CRediT authorship contribution statement

Jinzha Zhang: Carring out experiments and data curation, Writing – original draft. **Xuan Liu:** Data curation, Investigation. **Huaxiao Liu:** Data curation, Investigation. **Jingzhi Wang:** Data curation, Investigation. **Yawen Zhang:** Investigation. **Wenbo Zhao:** Funding acquisition, Resources, Writing – review & editing, Supervision, Project administration, all authors discussed the results and reviewed the manuscript.

Declaration of competing interest

The authors declare that they have no known competing financial interests or personal relationships that could have appeared to influence the work reported in this paper.

Data availability

No data was used for the research described in the article.

Acknowledgment

The work was supported by National Natural Science Foundation of China (No: 22175096), Social Development Project of Jiangsu Natural Science Foundation (No: BE2019744), Jiangsu Collaborative Innovation Center of Biomedical Functional Materials, the Priority Academic Program Development of Jiangsu Higher Education Institution.

Appendix A. Supplementary data

Supplementary data to this article can be found online at https://doi.org/10.1016/j.aca.2022.340251.

References

[1] A. Bansal, M.C. Simon, Glutathione metabolism in cancer progression and treatment resistance, J. Cell Biol. 217 (2018) 2291–2298.
[2] A. Malla, R.M. Umesh, S. Yousf, S. Mane, S. Sharma, M. Lahiri, P. Talukdar, A glutathione activatable ion channel induces apoptosis in cancer cells by depleting intracellular glutathione levels, Angew. Chem. Int. Ed. 59 (2020) 7944–7952.
[3] R.J. Mayer, A.R. Ofial, Nucleophilicity of glutathione: a link to michael acceptor reactivities, Angew. Chem. Int. Ed. 58 (2019) 17704–17708.
[4] X. Huang, F. Xia, Z.D. Nan, Fabrication of FeS_2/SiO_2 double mesoporous hollow spheres as an artificial peroxidase and rapid determination of H_2O_2 and glutathione, ACS Appl. Mater. Interfaces 12 (2020) 46539–46548.
[5] C. Kinoshita, K. Kikuchi-Utsumi, K. Aoyama, R. Suzuki, Y. Okamoto, N. Matsumura, D. Omata, K. Maruyama, T. Nakaki, Inhibition of miR-96-5p in the mouse brain increases glutathione levels by altering NOVA1 expression, Commun. Biol. 4 (2021) 182.
[6] S. Singh, S. Ghosh, V.K. Pal, M. Munshi, P. Shekar, D.T.N. Murthy, G. Mugesh, A. Singh, Antioxidant nanozyme counteracts HIV-1 by modulating intracellular redox potential, EMBO Mol. Med. 13 (2021), e13314.
[7] Z.Y. sun, C.J. Song, C. Wang, Y.Q. Hu, J.H. Wu, Hydrogel-based controlled drug delivery for cancer treatment: a review, Mol. Pharm. 17 (2020) 373–391.
[8] J.H. Bong, H.W. Song, T.H. Kim, M.J. Kang, J. Jose, J.C. Pyun, Refolding of autodisplayed anti-NEF scFv through oxidation with glutathione for immunosensors, Biosens. Bioelectron. 102 (2018) 600–609.
[9] M. Keshavarz, B. Tan, K. Venkatakrishnan, Label-free SERS quantum semiconductor probe for molecular-level and in vitro cellular detection: a noble-metal-free methodology, ACS Appl. Mater. Interfaces 10 (2018) 34886–34904.
[10] L.J. Ma, C. Buescchl, R. Schuhmacher, A.L. Waterhouse, Tracing oxidation reaction pathways in wine using C-13 isotopolog patterns and a putative compound database, Anal. Chim. Acta 1054 (2019) 74–83.
[11] J. Noh, B. Kwon, E. Han, M. Park, W. Yang, W. Cho, W. Yoo, G. Khang, D. Lee, Amplification of oxidative stress by a dual stimuli-responsive hybrid drug enhances cancer cell death, Nat. Commun. 6 (2015) 6907.
[12] D.K. Kwon, J.M. Myoung, Wearable and semitransparent pressure-sensitive light-emitting sensor based on electrochemiluminescence, ACS Nano 14 (2020) 8716–8723.
[13] Y. Wang, R. Jin, N. Sojic, D. Jiang, H.Y. Chen, Intracellular wireless analysis of single cells by bipolar electrochemiluminescence confined in a nanopipette, Angew. Chem. Int. Ed. 59 (2020) 10416–10420.
[14] A. Jones, L. Dhanapala, R.N.T. Kankanamage, C.V. Kumar, J.F. Rusling, Multiplexed immunosensors and immunoarrays, Anal. Chem. 92 (2020) 345–362.

[15] S. Tajik, Z. Dourandish, K. Zhang, H. Beitollahi, Q.V. Le, H.W. Jang, M. Shokouhimehr, Carbon and graphene quantum dots: a review on syntheses, characterization, biological and sensing applications for neurotransmitter determination, RSC Adv. 10 (2020) 15406–15429.

[16] N.N. Wang, H. Gao, Y.Z. Li, G.M. Li, W.W. Chen, Z.C. Jin, J.P. Lei, Q. Wei, H.X. Ju, Dual intramolecular electron transfer for in situ coreactant-embedded electrochemiluminescence microimaging of membrane protein, Angew. Chem. Int. Ed. 60 (2021) 197–201.

[17] Z.Y. Wang, J.B. Pan, Q. Li, Y. Zhou, S. Yang, J.J. Xu, D.B. Hua, Improved AIE-active probe with high sensitivity for accurate uranyl ion monitoring in the wild using portable electrochemiluminescence system for environmental applications, Adv. Funct. Mater. 30 (2020), 2000220.

[18] W.J. Niu, R.H. Zhu, S. Cosnier, X.J. Zhang, D. Shan, Ferrocyanide-ferricyanide redox couple induced electrochemiluminescence amplification of carbon dots for ultrasensitive sensing of glutathione, Anal. Chem. 87 (2015) 11150–11156.

[19] C. Han, W.W. Guo, Fluorescent noble metal nanoclusters loaded protein hydrogel exhibiting anti-biofouling and self-healing properties for electrochemiluminescence biosensing applications, Small 16 (2020) 1613–6829.

[20] X. Zhu, X. Zhang, Y. Zhou, Y. Chai, R. Yuan, High-efficient electrochemiluminescence of Au nanoclusters induced by the electrosensitizer Cu_2O: the mechanism insights from the electrogenerated process, Anal. Chem. 93 (2021) 10212–10219.

[21] B. Bansod, T. Kumar, R. Thakur, S. Rana, I. Singh, A review on various electrochemical techniques for heavy metal ions detection with different sensing platforms, Biosens. Bioelectron. 94 (2017) 443–455.

[22] Z. Farka, T. Juriik, D. Kovaar, L. Trnkova, P. Sklaadal, Nanoparticle-based immunochemical biosensors and assays: recent advances and challenges, Chem. Rev. 117 (2017) 9973–10042.

[23] M. Kukkar, G.C. Mohantaa, S.K. Tuteja, P. Kumar, A.S. Bhadwal, P. Samaddar, K. H. Kim, A. Deep, A comprehensive review on nano-molybdenum disulfide/DNA interfaces as emerging biosensing platforms, Biosens. Bioelectron. 107 (2018) 244–258.

[24] F. Andrea, I. null, V. Giovanni, P. Francesco, E. Yasuaki, Electrogenerated chemiluminescence with peroxydisulfate as a coreactant using boron doped diamond electrodes, Anal. Chem. 90 (2018) 12959–12963.

[25] S. Voci, R. Duwald, S. Grass, D.J. Hayne, L. Bouffier, P.S. Francis, J. Lacour, N. Sojic, Self-enhanced multicolor electrochemiluminescence by competitive electron-transfer processes, Chem. Sci. 11 (2020) 4508–4515.

[26] Z. Yiran, Y. Jing, X. Guobao, S. Neso, L. Gabriel, Photo-induced electrochemiluminescence at silicon electrodes in water, J. Am. Chem. Soc. 141 (2019) 13013–13016.

[27] R. Heidari, J. Rashidiani, M. Abkar, R.A. Taheri, M.M. Moghaddam, S. A. Mirhosseini, R. Seidmoradi, M.R. Nourani, M. Mahboobi, A.H. Keihan, H. Kooshki, CdS nanocrystals/graphene oxide-Au NPs based electrochemiluminescence immunosensor in sensitive quantification of a cancer biomarker: p53, Biosens, Bioelectron 126 (2019) 7–14.

[28] M. Hesari, K.N. Swanick, J.S. Lu, R. Whyte, S.N. Wang, Z.F. Ding, Highly efficient dual-color electrochemiluminescence from BODIPY-capped PbS nanocrystals, J. Am. Chem. Soc. 137 (2015) 11266–11269.

[29] X. Wang, H. Liu, H. Qi, Q. Gao, C. Zhang, Highly efficient electrochemiluminescence of ruthenium complex-functionalized CdS quantum dots and their analytical application, J. Mater. Chem. B 8 (2020) 3598–3605.

[30] L. Fu, B. Zhang, X.Y. Long, K. Fu, X.W. Gao, G.Z. Zou, Promising electrochemiluminescence from $CuInS_2$/ZnS nanocrystals/hydrazine via internal Cu (I)/Cu (II) couple cycling, Anal. Chem. 91 (2019) 10221–10226.

[31] Y.M. Lei, B.Q. Xiao, W.B. Liang, Y.Q. Chai, R. Yuan, Y. Zhuo, A robust, magnetic, and self-accelerated electrochemiluminescent nanosensor for ultrasensitive detection of copper ion, Biosens. Bioelectron. 109 (2018) 109–115.

[32] Y. Li, Y.X. Chu, Y.F. Li, C. Ma, L.L. Li, A novel electrochemiluminescence biosensor: inorganic-organic nanocomposite and $ZnCo_2O_4$ as the efficient emitter and accelerator, Sensor. Actuator. B Chem. 303 (2020), 127222.

[33] A. Yang, X. Huangfu, L. Liu, W. Luo, W. Zhao, J. Yin, Electrochemiluminescence immunosensor based on signal probe $CuFeS_2$ quantum dots for ultrasensitive detection of cyclin D1, J. Electroanal. Chem. 871 (2020), 114269.

[34] X. Long, X. Tan, Y. He, G. Zou, Near-infrared electrochemiluminescence from non-toxic $CuInS_2$ nanocrystals, J. Mater. Chem. C 5 (2017) 12393–12399.

[35] N. Liang, Q. He, S. Huang, M. Wang, W. Chen, M. Xu, Y. Yuan, J. Zai, N. Fang, X. Qian, AgInxGa1-xS_2 solid solution nanocrystals: synthesis, band gap tuning and photocatalytic activity, CrystEngComm 16 (2014) 10123–10130.

[36] S. Paderick, M. Kessler, T.J. Hurlburt, S.M. Hughes, Synthesis and characterization of $AgGaS_2$ nanoparticles: a study of growth and fluorescence, Chem. Commun. 54 (2018) 62–65.

[37] J. Song, Y. Zhang, Y. Dai, J. Hu, L. Zhu, X. Xu, Y. Yu, H. Li, B. Yao, H. Zhou, Polyelectrolyte-mediated nontoxic AgGaxIn1-xS_2 QDs/low-density lipoprotein nanoprobe for selective 3D fluorescence imaging of cancer stem cells, ACS Appl. Mater. Interfaces 11 (2019) 9884–9892.

[38] F. Huang, J. Zhou, J. Xu, Y. Wang, Formation of $AgGaS_2$ nano-pyramids from Ag_2S nanospheres through intermediate Ag_2S-$AgGaS_2$ heterostructures and $AgGaS_2$ sensitized Mn^{2+} emission, Nanoscale 6 (2014) 2340–2344.

[39] N.S. Adamson, A.G. Theakstone, L.C. Soulsby, E.H. Doeven, E. Kerr, C.F. Hogan, P. S. Francis, L. Dennany, Emission from the working and counter electrodes under co-reactant electrochemiluminescence conditions, Chem. Sci. 12 (2021) 9770–9777.

[40] W. Wang, Y. Liu, T. Shi, J. Sun, F. Mo, X. Liu, Biosynthesized quantum dot for facile and ultrasensitive electrochemical and electrochemiluminescence immunoassay, Anal. Chem. 92 (2020) 1598–1604.

[41] S. Fernandez-Poza, A. Padros, R. Thompson, L. Butler, M. Islam, J.A. Mosely, J. H. Scrivens, M.F. Rehman, M.S. Akram, Tailor-made recombinant prokaryotic lectins for characterisation of glycoproteins, Anal. Chim. Acta 1155 (2021), 338352.

[42] K. Nawara, J. Waluk, Goodbye to quinine in sulfuric acid solutions as a fluorescence quantum yield standard, Anal. Chem. 91 (2019) 5389–5394.

[43] Q. Zhou, S.Z. Kang, X. Li, L. Qin, J. Mu, $AgGaS_2$ nanoplates loaded with CuS: an efficient visible photocatalyst for rapid H_2 evolution, Int. J. Hydrogen Energy 40 (2015) 4119–4128.

[44] C.M. Fan, M.D. Regulacio, C. Ye, S.H. Lim, Y.G. Zheng, Q.H. Xu, A.W. Xu, M. Y. Han, Colloidal synthesis and photocatalytic properties of orthorhombic $AgGaS_2$ nanocrystals, Chem. Commun. 50 (2014) 7128–7131.

[45] X. Yang, N. Zhao, Q. Zhou, C. Cai, X. Zhang, J. Xu, Precise preparation of highly monodisperse ZrO_2@SiO_2 core-shell nanoparticles with adjustable refractive indices, J. Mater. Chem. C 1 (2013) 3359–3366.

[46] L. Dennany, M. Gerlach, S. O'Carroll, T.E. Keyes, R.J. Forster, P. Bertoncello, Electrochemiluminescence (ECL) sensing properties of water soluble core-shell CdSe/ZnS quantum dots/Nafion composite films, J. Mater. Chem. 21 (2011) 13984–13990.

[47] X. Zhang, F.G. Wu, P. Liu, N. Gu, Z. Chen, Enhanced fluorescence of gold nanoclusters composed of $HAuCl_4$ and histidine by glutathione: glutathione detection and selective cancer cell imaging, Small 10 (2014) 5170–5177.

[48] Y.W. Bao, X.W. Hua, J. Zeng, F.G. Wu, Bacterial template synthesis of multifunctional nanospindles for glutathione detection and enhanced cancer-specific chemo-chemodynamic therapy, Research 2020 (2020), 9301215.

[49] Y. Guo, X. Zhang, F.G. Wu, A graphene oxide-based switch-on fluorescent probe for glutathione detection and cancer diagnosis, J. Colloid Interface Sci. 530 (2018) 511–520.

[50] H. Wang, R. Zhang, Y. Zhuo, R. Yuan, Sensitive electrochemiluminescence biosensor for glutathione using MnO_2 nanoflower as novel co-reaction accelerator for Ru complex/tripropylamine system, Anal. Chim. Acta 1188 (2021), 339181.

[51] T. Han, J. Yang, Y. Wang, Y. Cao, Y. Wang, H.Y. Chen, J.J. Zhu, Boosted anodic electrochemiluminescence from blue-emissive sulfur quantum dots and its bioanalysis of glutathione, Electrochim. Acta 381 (2021), 138281.

[52] H.P. Peng, M.L. Jian, Z.N. Huang, W.J. Wang, H.H. Deng, W.H. Wu, A.L. Liu, X. H. Xia, W. Chen, Facile electrochemiluminescence sensing platform based on high-quantum-yield gold nanocluster probe for ultrasensitive glutathione detection, Biosens. Bioelectron. 105 (2018) 71–76.

[53] Y.H. Seo, T. Kim, C.K.P. Truong, H.S. No, J.I. Hong, I.S. Shin, Electrochemiluminescent "turn-on" chemosensor based on the selective recognition binding kinetics with glutathione, Sensor. Actuator. B Chem. 357 (2022), 131408.